Microfluid Nanofluid (2013) 14:943–950
DOI 10.1007/s10404-012-1101-9

RESEARCH PAPER

Time-resolved electrochemical measurement device for microscopic liquid interfaces during droplet formation

Mao Fukuyama · Yumi Yoshida · Jan C. T. Eijkel · Albert van den Berg · Akihide Hibara

Received: 29 February 2012 / Accepted: 9 May 2012 / Published online: 11 December 2012

Abstract An electrochemical measurement system with a high-speed camera for observation of dynamic behavior of ionic molecules at a water-in-oil interface during microfluidic droplet formation is described. In order to demonstrate the usefulness of the system, a liquid interface between 1 M sodium chloride aqueous solution and 0.02 M tetrabutylammonium tetraphenylborate 1,2-dichloroethane solution was investigated. During aqueous droplet formation in a microfluidic device, averaged and dynamic currents between the two phases were measured under potential control. The measured current corresponded to the transport of electrolyte ions to form the electrical double layer at the liquid interface. When an 18-μm-sized droplet was formed in each 1.2 ms, the amount of charge on each droplet was measured to be 20 pC at 0.4 V and negligible at the potential of zero charge (0.19 V). In addition, the high-speed camera observations revealed that the charge affects the stability of the droplet during and/or just after the generation process. This measurement system is expected to facilitate a fuller understanding of the droplet formation process.

M. Fukuyama · A. Hibara (✉)
Institute of Industrial Science, The University of Tokyo, 4-6-1 Komaba, Meguro-ku, Tokyo 153-8505, Japan
e-mail: hibara@iis.u-tokyo.ac.jp

Y. Yoshida
Department of Chemistry and Material Technology, Kyoto Institute of Technology, Hashikamicho Matsugasaki, Sakyo-ku, Kyoto 606-0951, Japan

J. C. T. Eijkel · A. van den Berg
MESA+ Institute for Nanotechnology, University of Twente, PO Box 217, 7500 AE Enschede, The Netherlands

Keywords Microfluidics · Electrochemical measurement · Microdroplet formation · Liquid/liquid interface

Abbreviations

DCE	1,2-Dichloroethane
NaCl	Sodium chloride
PZC	Potential of zero charge
TBATPB	Tetrabutylammonium tetraphenylborate
TBACl	Tetrabutylammonium chloride

1 Introduction

Research into the miniaturization of chemical and biochemical processes on microfabricated devices has been advancing rapidly (West et al. 2008; Günther and Jensen 2006). Recently, droplets generated in microdevices have attracted much attention as a novel fluid operation field (Teh et al. 2008). The droplets can encapsulate materials in volumes as small as a femtoliter or picoliter (Tan et al. 2006), and be separated (Link et al. 2004), sorted (Maenaka et al. 2008), fused (Tan and Takeuchi 2006), and inverted (Fukuyama and Hibara 2011) by utilizing the microchannel structure and wettability. Various biochemical analyses and material syntheses have been demonstrated in the field (Huebner et al. 2008; Song et al. 2006; Shui et al. 2007).

Precision of volume is one of the most distinctive features of droplet operation, and understanding of the formation process is a key topic in the field. In order to analyze the formation process, it is necessary to measure the micrometer-sized droplet formation on a millisecond time scale, and high-speed camera observation has often been applied (Christopher and Anna 2007). According to the results of various investigations, it was found that the

capillary number, a dimensionless number for the ratio of viscous force to interfacial tension, is one of the important parameters that determine the droplet size (Zheng et al. 2004; Sugiura et al. 2002). On the other hand, droplet sizes are also known to depend on surfactant species, even when having the same capillary number (Shui et al. 2009). Therefore, the physicochemical parameters of the interface (e.g., interfacial tension, specie of surfactant, and channel wall wettability) need be taken into account in any investigation of droplet formation.

In conventional studies, despite the dynamic nature of the formation process, static interfacial parameters have been used. For instance, the interfacial tension during droplet formation is higher than in the equilibrium state, because of the kinetic surfactant adsorption to the interface (Sugiura et al. 2001a). The adsorption process is determined mainly by diffusive and convectional transport and kinetic adsorption/desorption. By taking these phenomena into account, transient and variable water-in-oil (W/O) interfacial tension affects the droplet formation dynamics (Baret 2012).

Thus, real-time, interface-selective and on-site measurement methods for determining interfacial properties are required in order to achieve a fuller understanding of the droplet formation process. Several methods for evaluating dynamic or static interfacial tension in microfabricated devices have been reported (Steegmans et al. 2009; Xu et al. 2008; Wang et al. 2009). These methods, however, can be applied only to the droplet formation process with a simple assumption: for example, they cannot explain the dependence of size on surfactant species. Therefore, a direct measurement approach based on molecular kinetics would be extremely desirable.

In order to discuss molecular behavior at the interface during droplet formation, we focused on electrochemical measurement at a liquid/liquid interface. The electrochemical measurement has sufficient resolution to measure the kinetics of ions in a μm^2-sized interface (Taylor and Girault 1986; Osborne et al. 1994) within a millisecond. In addition, electrochemical measurement is expected to measure not only the transportation of ion and ionic surfactant to the interface (Goto et al. 2005), but also the amount of adsorbed nonionic surfactant, indirectly by measurement of capacitance (Chen et al. 1991). From the viewpoint of conventional electrochemical methods, molecular kinetics at the W/O interface during droplet formation have been well investigated in polarography with the interface between two immiscible electrolyte solutions (Kihara et al. 1986; Reymond et al. 2000). Some polarography setups using mm-sized droplets formed on a time scale of tens of milliseconds have been reported (Bond and O'Halloran 1976). In order to discuss the microfluidic droplet formation processes, a new analytical device for the molecular behavior is required.

In this paper, an electrochemical measurement system for analyzing the droplet formation process in a microfluidic device is reported. The main example of molecular kinetics affecting an interfacial property during droplet formation was the measurement of the ion transport phenomena creating an electrical double layer at an aqueous/1,2-dichloroethane (DCE) interface. The dependence of the amount of charge accumulating in the electrical double layer on the potential between two liquids was observed, and its relation to the stability of the droplet is discussed below.

2 Experimental section

2.1 Chemicals

Supporting electrolytes for aqueous and organic phases were NaCl (Wako Chemicals Co., Ltd., Osaka, Japan) and tetrabutylammonium tetraphenylborate (TBATPB; Tokyo Chemical Industry Co., Ltd., Tokyo, Japan). DCE (Wako chemicals Co., Ltd., Osaka, Japan) was used as organic phase. An aqueous solution of tetrabutylammonium chloride (TBACl; Sigma Aldrich, Japan; K. K., Tokyo, Japan) was used as reference/counter electrode for the organic phase. All the aqueous solutions were prepared with Milli-Q water. Octadecyltrichlorosilane (Sigma Ardrich Japan K. K., Tokyo, Japan), a silane-coupling reagent, was used for microchannel wall modification. These chemicals were used without any purification. Ag/AgCl electrodes were prepared on an Ag wire ($\phi = 200$ μm) in the 1 M NaCl aqueous solution by the electrodeposition.

Although surfactant plays an essential role in droplet formation, surfactant was not added to the system, in order to demonstrate the effectiveness of the present setup in the observation of dynamic ion accumulation in the electrical double layer during droplet formation.

2.2 Fabrication

Glass microfluidic devices were fabricated using a two-step photolithography and wet-etching technique (Hibara et al. 2005). The layout of the microchannel is shown in Fig. 1a. The black lines indicate the microchannels fabricated on the bottom glass plate, and the red circles correspond to 0.5-mm-diameter holes drilled through the top glass plate. The top and bottom plates were thermally bonded.

In the layout, the top and next to top holes on the left were used as aqueous and organic inlets, respectively. Immediately after the inlets, deep winding channels were fabricated in the wide shallow etched area in order to trap small particles at this stage and to prevent them contaminating the droplet formation. Following this filtration

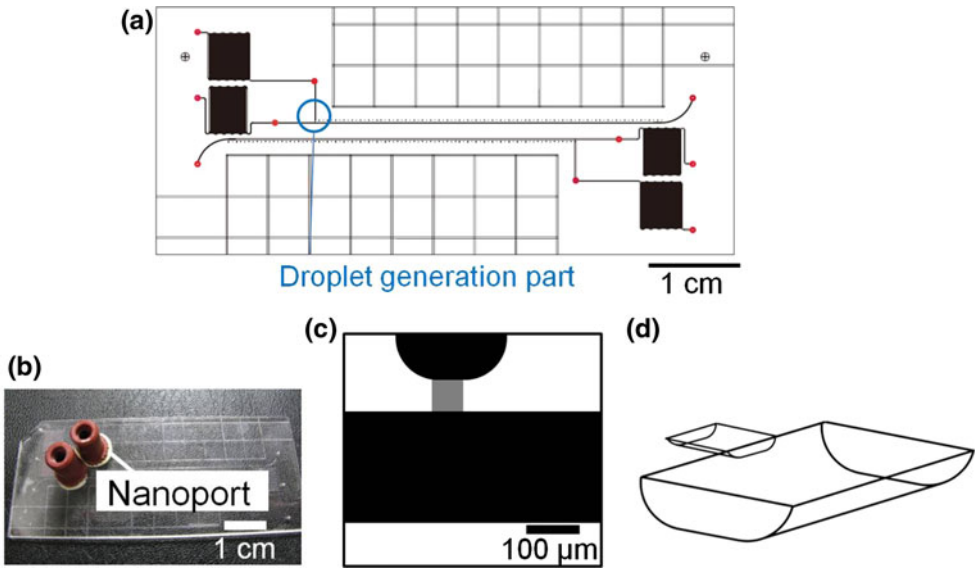

Fig. 1 Glass microfluidic device for electrochemical measurement at a W/O interface during droplet formation. **a** Layout of microchannel. *Red circles* indicate holes drilled for liquid introduction and electrode connection. **b** Photograph of the device. **c** Expanded view of the droplet formation section. The *black* and *gray areas* correspond to the deep channels and shallow part, respectively. **d** Three-dimensional view of the droplet formation section

procedure, the two channels enter the droplet formation section. Before the entry point, electrode connection ports (the red circles in the midway of the channels) were prepared by attaching Nanoports (Upchurch Scientific Inc., USA) to the top glass plate (Fig. 1b). The design of the droplet formation section is illustrated in Fig. 1c, d. The horizontal main channel and the vertical side channels were connected through the shallow channel (the gray area in Fig. 1c). When the aqueous and organic phases were allowed to flow from the side and main channels, respectively, aqueous droplets were formed at the junction of the main and shallow channels.

Using the same basic layout, two devices (device 1 and 2) were prepared. In device 1, the main and side channels had a width of 200 μm and a depth of 40 μm, while the shallow part had a width of 60 μm and a depth of 2 μm. In device 2, the main and side channels had a width of 200 μm and a depth of 50 μm, while the shallow part had a width of 60 μm and a depth of 6 μm. Device 1 was used for cyclic voltammetry measurements at the static (without flow) interface, and device 2 was used for the electrochemical and high-speed camera measurement during droplet formation. The microchannel wall surface was modified with an octadecylsilane group (Hibara et al. 2005).

2.3 Observation setup

Two syringe pumps (Model 210, KD Scientific Inc., USA) were used to introduce solutions to the microdevice. The droplet formation process was observed by an inverted microscope (IX71, Olympus Optical Co. Ltd., Japan) with a high-speed camera (FASTCAM SA3, Photoron Co. Ltd., Japan) at a frame rate of 5,000 fps. A potentiostat (electrochemical analyzer) (HZ-5000, Hokuto Denko Co. Ltd., Japan) was used for cyclic voltammetry and amperometry. The scan rates of cyclic voltammetry at the interface in a conventional bulk setup and in the microchannel setup were 20 and 500 mV/s, respectively. In the amperometric measurement, the current was recorded for 100 ms with a sampling rate of 50 kHz.

2.4 Preparation of electrochemical measurement

The electrochemical cell in this paper is shown below.

$$\text{Ag}|\text{AgCl}|\,0.02\text{M TBACl aq.}\,|\,0.02\text{M TBATPB in DCE}\,|\,1\text{M NaCl aq.}\,|\text{AgCl}|\text{Ag} \quad (1)$$

The Ag/AgCl electrode was immersed in TBACl aq., and the aqueous phase was used as the counter/reference (CE/RE) electrode for the organic phase. The potential between the organic phase and TBACl aq. was determined by the TBA ion transfer. After filling the main channel with TBATPB org., TBACl aq. pool was prepared in the Nanoport of the organic side and the Ag/AgCl electrode was inserted. An Ag/AgCl working electrode (WE) was set to the Nanoport of the aqueous side after introducing NaCl aq. to the side channel and Nanoport (Fig. 2a). As the result of this procedure, the W/O interface was prepared in the shallow channel.

The device was set in a homemade Faraday cage that has windows for observation (Fig. 2b). All the connectors and capillaries were wrapped in aluminum foil that was in contact with the Faraday cage. The solution resistance in each device was calculated using data from the literature (Vanysek et al. 1990). The resistances in devices 1 and 2 were calculated as 15 and 13 MΩ, respectively, when the shallow channel was assumed to be filled with the aqueous solution.

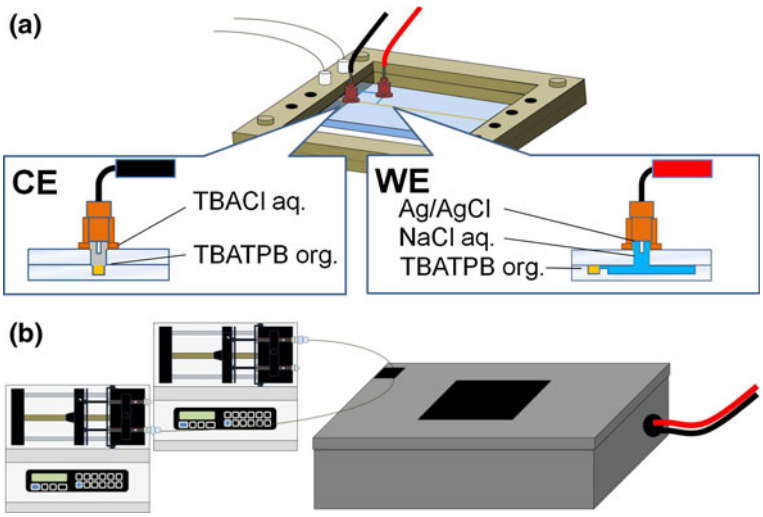

Fig. 2 Experimental setup. **a** Schematic illustration of liquid capillary connection and electrode preparation. **b** Overview of the setup. The microdevice was contained in a homemade Faraday cage

A centimeter-sized W/O interface set in a cylindrical batch with a diameter of 4.5 cm was measured in order to evaluate the results of measurement in the microdevice. The electrochemical cell is shown below.

$$\text{Ag}|\text{AgCl}|\,0.02\text{M TBACl aq.}\,|\,0.02\text{M TBATPB in DCE}|\,1\text{M NaCl aq.}\,|\text{AgCl}|\text{Ag} \quad (2)$$

In addition to Eq. 2, a Pt counter electrode was inserted in the organic phase.

3 Results and discussion

3.1 Cyclic Voltammetry

Before measurements were made in the microchannel, a voltammogram was recorded in the centimeter-scale interface (Fig. 3a). A positive current appearing over 0.42 V indicates the transfer of a cation from the aqueous phase to the organic phase and/or of an anion in the opposite direction (Senda et al. 1991). In the present case, the positive current corresponds to TPB^- transfers from DCE to the aqueous phase and/or Na^+ transfers from the aqueous phase to DCE. The negative current around 0.42 V during the potential reducing scan indicates the return of TPB^- to DCE and/or to the aqueous phase. In the same manner, the negative current appearing under −0.02 V is attributed to TBA^+ transfers from DCE to the aqueous phase and/or Cl^- transfers from the aqueous phase to DCE. The positive current appearing during the potential increasing scan indicates the return of TBA^+ to DCE and/or Cl^- to the aqueous phase. In the potential window between −0.02 and 0.42 V, no ion was transferred and only the charging current to form the electrical double layer at the interface was measured. The potential of zero

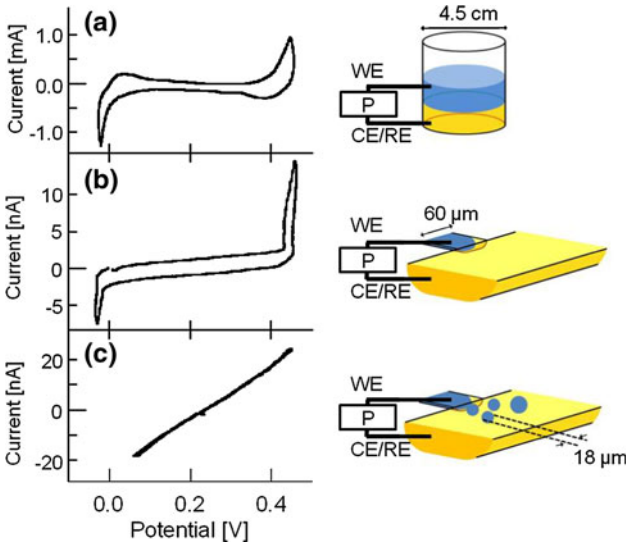

Fig. 3 Cyclic voltammograms at the W/O interface. The scan rates in a centimeter-scale cell and in the microchannel setup were 20 and 500 mV/s, respectively. **a** Static interface at the centimeter-scale cell. **b** Static interface in the microchannel. **c** Interface during droplet formation with a frequency of 1,000 Hz. The flow rates for the aqueous (dispersed) and organic (continuous) phases were set to 0.25 and 0.5 μL/min, respectively

charge (PZC) was determined as 0.19 V by a quasi-elastic laser scattering method (Nagatani et al. 2003; Hibara et al. 2003). The ion-transfer potentials are determined by the concentrations and species of the ions.

The voltammogram measured in the microdevice is shown in Fig. 3b. The ion-transfer currents measured were in the same potential range as in the centimeter-sized measurement. This result confirms that the target W/O interface in the microchannel was correctly measured by the present system. Because of faster diffusion, the current peaks corresponding to the ion return were not observed in the microchannel.

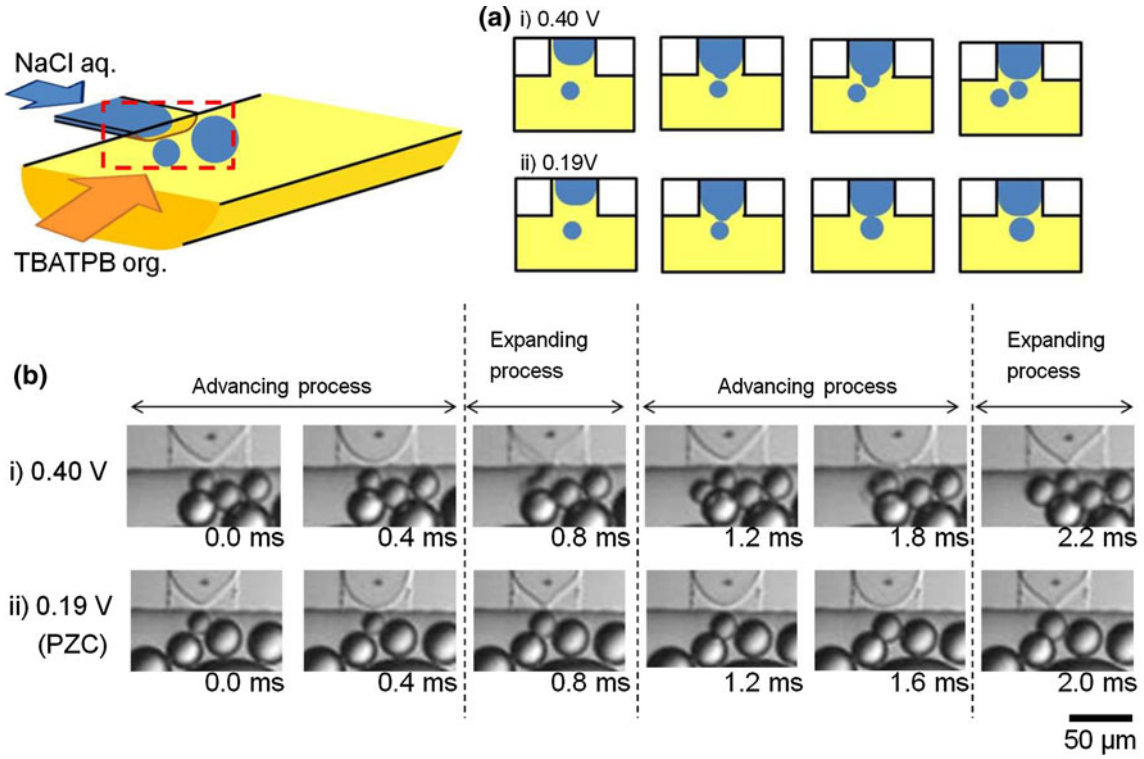

Fig. 4 Droplet formation in the microdevice. **a** Illustrations of droplet formation at each potential. While a new droplet is formed at 0.4 V, the liquid in the shallow channel connects to a previously generated droplet at 0.19 V. **b** Micrographs of droplet formation at each potential captured by high-speed camera. Flow rates of the dispersed and continuous phases were 0.25 and 0.5 μL/min, respectively

In contrast, the voltammogram measured during droplet formation had a very different shape compared to that of the static W/O interface (Fig. 3c). A characteristic linear-shaped voltammogram was obtained and no plateau window was observed. This unexpected shape is explained below, considering the dynamic process during droplet formation.

3.2 Microscopic observation

With the flow rates of the dispersed and continuous phases set to 0.25 and 0.5 μL/min, respectively, the droplets were generated with a frequency around 1,000 Hz. From the high-speed camera observations, the droplet formation process was found to depend on the applied potential.

At a potential of 0.40 V, when a new droplet was generated from the tip of the dispersed phase, the new droplet repels the previously generated droplet to form a single droplet, as shown in Fig. 4a (i). A series of micrographs of the droplet formation process is shown in Fig. 4b (i). The formation process in this device is similar to that reported by Sugiura et al. (2001b).

Here, the mechanism of droplet formation is described briefly. The dispersed (aqueous) phase that advances in the hydrophobic shallow channel (Fig. 4a left) has a relatively high Laplace pressure due to the small curvature radius. Next, when the front line (the tip) reaches the boundary between the shallow and main channels, the tip of the dispersed phase expands and forms a drop shape. At this time, the pressure required to form a spherical drop in the main channel is lower than that required to proceed or stay in the shallow channel. Then, the front line of the dispersed phase in the shallow channel recedes and the receded volume flows into the expanding drop. The liquid junction between the dispersed phase in the shallow channel and that in the main channel is thinned by the receding of the front line, and the drop in the main channel detaches from the dispersed phase in the shallow channel. In the case of the potential of 0.40 V, the liquid interface is sufficiently repulsive to that of the previously generated droplet. Thus, a new droplet is formed without fusion to the previously generated droplet.

In contrast, when the potential is set around the PZC, the tip of the dispersed phase connects and fuses with the previously generated droplet near the junction, and the volume of the droplet increases, as shown in Fig. 4a (ii), b (ii). Conventionally, the difference in droplet stability is explained simply by static interfacial tension. However, the

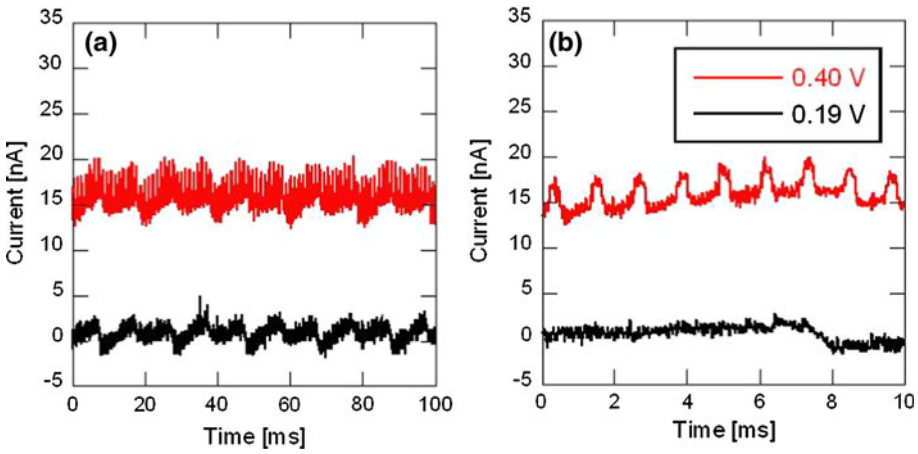

Fig. 5 Amperogram during droplet formation (**a**) and expanded view (**b**). Artifacts due to the line noise of 50 Hz are observed in both potentials. The period of the variation of 800 Hz at 0.4 V corresponds to single droplet formation. The current increases when the interface expands and falls when the droplet is detached from the dispersed phase

values of interfacial tension are 26 mN/m for 0.40 V and 28 mN/m for 0.19 V, and this difference cannot explain the results. Therefore, the processes have to be analyzed in terms of the amount of dynamic interfacial charge.

3.3 Amperometric measurement

Figure 5a shows the results of amperometric measurement at 0.40 V and 0.19 V during droplet formation, while Fig. 5b shows their expanded views. The time course of 0.40 V consists mainly of two components: a background and a periodic temporal variation. In contrast, the time course of 0.19 V does not have the variation and the background. Artifacts due to the line noise of 50 Hz are observed at both potentials.

The period of the variation of 800 Hz at 0.40 V corresponds to single droplet formation, which was also validated by the high-speed camera observation. The current increase and drop in the period correspond to the droplet expansion and its detachment, respectively. Since the ion cannot be transported across the interface at 0.40 V, the observed current corresponds to the charging of the ions to form the electrical double layer. However, compared with the cyclic voltammogram of the static interface (Fig. 3b), a higher background current was observed. This phenomenon can be explained when a simple series resistor–capacitor (RC) equivalent circuit is assumed. Just after a droplet is detached, the interface is an almost empty condenser. The initial current to the empty condenser was estimated as 16 nA, which approximately agrees with the observed current (14 nA). Contrastively, the charging current was almost zero at PZC since the interface cannot be charged up at this potential.

Although the current in an RC series circuit decreases with time, in this measurement setup, the current not only failed to decrease during the advancing process but also increased during the expanding process. This can be explained as follows.

Charging current relaxation The capacitance of the present device 2 (C) was calculated as 6 nF from the current at PZC (1 nA) in Fig. 3b, and the scan rate (500 mV/s), where the ratio of the shallow channel depth of the present device 2 (6 μm) to that of device 1 (2 μm), was considered. The relaxation time (RC) was estimated to be around 80 ms, and the current relaxation during 1 ms was about 1 %.

Resistance deviation due to the advance of the dispersed phase in the shallow channel As described above, the front line of the dispersed phase recedes during the expansion of the drop. The receded volume is filled with the organic phase, which has higher resistivity (24 Ω/m) than the aqueous phase (0.12 Ω/m). When 10-μm receding is assumed, the total resistance of the system is 13.6 MΩ. During the advancing process, the resistance becomes 13.0 MΩ. The reduction of the resistance corresponds to a 4 % increase in current and it may compensate for the current decrease due to the relaxation.

The change in interface area during the expansion During the expanding process, the capacitance increase caused by the expansion of the interface leads to the increase in current that is clearly observed in the latter half of the period. As discussed above, the time course includes many processes. Since quantitative calculations of the time course of the current require deeper discussion and are beyond the scope of the present paper, they will be discussed in another work.

The characteristic ohmic-like behavior in Fig. 3c can be explained by considering the droplet formation process. The average of the transient current shown in Fig. 5 has good correlation with the current in the voltammogram shown in Fig. 3c. In the static voltammogram, the current measured is due to the deviation in the charge during the potential scan. In contrast, in the case of droplet formation, a fresh interface is always generated and only the initial stage of the charging is observed. Since the main component of the

current (the initial charging current) is linearly dependent on the potential from PZC, the voltammogram is approximately proportional to the potential. In the cyclic voltammogram, however, the current change corresponding to the different droplet formation mechanism was not observed. It can be considered that the change was too small to be observed at this measurement, since the absolute value of the current is small around PZC.

Next, the amount of charge at the electrical double layer was calculated in order to consider the droplet stability difference observed in Fig. 4. As seen in Fig. 5a, the averaged current was almost stationary during the continuous droplet formation. Therefore, it seems reasonable that the detached droplet carries the charge that accumulates during its formation (the time integral of the current). The charge at 0.40 V was calculated as 20 pC while that at 0.19 V was negligibly small (<1 pC). Since the surface area of the droplet is 3 times larger than that in the shallow channel, the capacity of the droplet is assumed to be 20 nF. The excess charge of 20 pC is <1 % of the fully charged value ($Q = CV$, where Q is the charge amount, and V is the potential deviation from PZC). When the excess charge is assumed to be maintained to generate a two-phase potential difference ($V = Q/C$), the difference is 1 mV. Before reaching the relaxed state, a higher potential difference is assumed to remain transiently at the interface. The difference can be considered to represent an electrical double layer around a droplet, which generates a repulsive force against the other droplet to prevent fusion.

The present measurements demonstrate the direct observation of molecular kinetics at the interface during microfluidic droplet generation. This electrochemical measurement system may have great potential for measuring the dynamic interfacial properties that cannot be evaluated by high-speed camera observation alone.

4 Conclusion

In this paper, we present an electrochemical measurement system for observing kinetics of ionic molecular at the W/O interface during droplet formation. By using this system, we measured the amount of charge at the interface of a single droplet as an example of the molecular behavior that affects droplet stability during its formation. We expect this measurement system to allow the observation of surfactant adsorption at the interface, revealing the time course of interfacial properties during droplet formation in microdevices, and leading to a fuller understanding of the phenomenon.

Acknowledgments We sincerely acknowledge Prof. Noritada Kaji, Prof. Yoshinobu Baba of Nagoya University, Mr. Rerngchai Arayanarakool and Dr. ir. Séverine le Gac of University of Twente for their kind support. We express gratitude to Prof. Kohji Maeda of Kyoto Institute of Technology for the helpful discussions and to Prof. Tetsu Tatsuma and Dr. Nobuyuki Sakai of the University of Tokyo for support regarding the electrochemical measurement. This work was partially supported by KAKENHI (Grant 23655064) and by the Food Nanotechnology Project of the Ministry of Agriculture, Forestry and Fisheries of Japan. MF acknowledges the Global COE Program, Chemistry Innovation through Cooperation of Science and Engineering, MEXT, Japan and the International Training Program, Program for incubating young researchers on Plasma Nanotechnology Materials and Device Processing, JSPS for encouragement of research activities.

References

Baret J-C (2012) Surfactants in droplet-based microfluidics. Lab Chip 12:422–433

Bond AM, O'Halloran RJ (1976) Pseudo-derivative D.C. and pulse polarographic methods at short drop time. J Electroanal Chem 68:257–272

Chen Q, Iwamoto K, Seno M (1991) Adsorption of poly(oxyethylene)dodecyl ethers at the water-nitrobenzene interface. Electrochim Acta 36:1437–1442

Christopher GF, Anna SL (2007) Microfluidic methods for generating continuous droplet streams. J Phys D Appl Phys 40:R319–R336

Fukuyama M, Hibara A (2011) Release of encapsulated content in microdroplets. Anal Sci 27:671–672

Goto T, Maeda K, Yoshida Y (2005) Relationship between interfacial transfer and adsorption-desorption of surface-active bis-ammonium ions at a liquid/liquid interface. Langmuir 21:11788–11794

Günther A, Jensen KF (2006) Multiphase microfluidics: from flow characteristics to chemical and materials synthesis. Lab Chip 6:1487–1503

Hibara A, Nonaka M, Tokeshi M, Kitamori T (2003) Spectroscopic analysis of liquid/liquid interfaces in multiphase microflows. J Am Chem Soc 125:14954–14955

Hibara A, Iwayama S, Matsuoka S, Ueno M, Kikutani Y, Tokeshi M, Kitamori T (2005) Surface modification method of microchannels for gas–liquid two-phase flow in microchips. Anal Chem 77:943–947

Huebner A, Sharma S, Srisa-Art M, Hollfelder F, Edel JB, deMello AJ (2008) Microdroplets: a sea of applications? Lab Chip 8:1244–1254

Kihara S, Suzuki M, Maeda K, Ogura K, Umetani S, Matsui M, Yoshida Z (1986) Fundamental factors in the polarographic measurement of ion transfer at the aqueous/organic solution interface. Anal Chem 58:2954–2961

Link DR, Anna SL, Weitz DA, Stone HA (2004) Geometrically mediated breakup of drops in microfluidic devices. Phys Rev Lett 92:1–4

Maenaka H, Yamada M, Yasuda M, Seki M (2008) Continuous and size-dependent sorting of emulsion droplets using hydrodynamics in pinched microchannels. Langmuir 24:4405–4410

Nagatani H, Fermi DJ, Girault HH (2003) Adsorption and aggregation of meso-tetrakis (4-carboxyphenyl) porphyrinato Zinc (II) at the polarized water|1,2-dichloroethane interface. J Phys Chem 107: 786–790

Osborne MC, Shao Y, Pereira CM, Girault HH (1994) Micro-hole interface for the amperometric of ionic species in aqueous solutions determination. J Electroanal Chem 364:155–161

Reymond F, Fermın D, Lee HJ, Girault HH (2000) Electrochemistry at liquid/liquid interfaces: methodology and potential applications. Electrochim Acta 45:2647–2662

Senda A, Kakiuchi T, Osakai T (1991) Electrochemistry two immiscible at the interface between electrolyte solutions. Electrochim Acta 36:253–262

Shui L, Eijkel JCT, van den Berg A (2007) Multiphase flow in microfluidic systems—control and applications of droplets and interfaces. Adv Coll Int Sci 133:35–49

Shui L, van den Berg A, Eijkel JCT (2009) Interfacial tension controlled W/O and O/W 2-phase flows in microchannel. Lab Chip 9:795–801

Song H, Chen DL, Ismagilov RF (2006) Reactions in droplets in microfluidic channels. Angew Chem Int Ed 45:7336–7356

Steegmans MLJ, Warmerdam A, Schroën KGPH, Boom RM (2009) Dynamic interfacial tension measurements with microfluidic Y-junctions. Langmuir 25:9751–9758

Sugiura S, Nakajima M, Ushijima H, Yamamoto K, Seki M (2001a) Preparation characteristics of monodispersed water-in-oil emulsions using microchannel emulsification. J Chem Eng Japan 34:757–765

Sugiura S, Nakajima M, Iwamoto S, Seki M (2001b) Interfacial tension driven monodispersed droplet formation from microfabricated channel array. Langmuir 17:5562–5566

Sugiura S, Nakajima M, Kumazawa N, Iwamoto S, Seki M (2002) Characterization of spontaneous transformation-based droplet formation during microchannel emulsification. J Phy Chem B 106:9405–9409

Tan W, Takeuchi S (2006) Timing controllable electrofusion device for aqueous droplet-based microreactors. Lab Chip 6:757–763

Tan Y, Hettiarachchi K, Siu M, Pan Y, Lee AP (2006) Controlled microfluidic encapsulation of cells, proteins, and microbeads in lipid vesicles. J Am Chem Soc 128:5656–5658

Taylor G, Girault HH (1986) Ion transfer reactions across a liquid–liquid interface supported on a micropipette tip. J Electroanal Chem 208:179–183

Teh S, Lin R, Hung L, Lee AP (2008) Droplet microfluidics. Lab Chip 8:198–220

Vanysek P, Hernandez IC, Xu J (1990) Supporting electrolytes for electrochemistry at liquid/liquid interfaces: crystal violet and tetrabutylammonium tetraphenylborate in nitrobenzene. J Colloid Interface Sci 139:527–534

Wang K, Lu YC, Xu JH, Luo GS (2009) Determination of dynamic interfacial tension and its effect on droplet formation in the T-shaped microdispersion process. Langmuir 25:2153–2158

West J, Becker M, Tombrink S, Manz A (2008) Micro total analysis systems: latest achievements. Anal Chem 80:4403–4419

Xu JH, Li SW, Lan WJ, Luo GS (2008) Microfluidic approach for rapid interfacial tension measurement. Langmuir 24:11287–11292

Zheng B, Tice JD, Ismagilov RF (2004) Formation of droplets of alternating composition in microfluidic channels and applications to indexing of concentrations in droplet-based assays. Anal Chem 76:4977–4982